

Computational exploration of Casson fluid flow over a Riga-plate with variable chemical reaction and linear stratification

Parasuraman Loganathan, Krishnamurthy Deepa

Department of Mathematics, Anna University,
Chennai, Tamilnadu, India
logu@annauniv.edu; deepakkrish1@gmail.com

Received: March 4, 2019 / Revised: May 3, 2019 / Published online: May 1, 2020

Abstract. Simulation of electro-magneto-hydrodynamic Casson fluid flow subject to cross stratification and variable chemical reaction is exemplified numerically. The model, which is governed by the system of partial differential equations, accomplishes the implicit finite difference solution. The variable chemical reaction enables the study to investigate an exponentially varying reaction rate along the stratified flow. Further, the mesh-contour plots impart the precise visualization of flow field in 3D and its projection as contour on XY -plane. The stronger chemical reaction parameter improves the temperature and mass transfer rate. The consistency of the results is affirmed by the correlation with results arising in the literature.

Keywords: EMHD Casson fluid, mesh-contour plot, variable chemical reaction, stratification.

1 Introduction

Chemical reaction modifies the amount of chemical components in a composition. It cannot be measured as a spatial phenomenon. Only the internal structure is repositioned, while the chemical bond between atoms has broken. The order of chemical reaction is one of the prominent features, which affect the rate of reaction. Because, the molecularity of elementary reaction rely on collision of molecules. Heat and mass transfer subject to chemical reaction can be utilized in execution of enormous engineering practices, namely, drying, temperature and moisture distribution in processing industries (Erdi et al. [8]). Many mathematical models have been evolved with the effects of chemical reaction, thermal and mass diffusivity. Das et al. [6] found the exact solution of chemically reacting viscous fluid flow on a vertical plate. Muthucumaraswamy and Ganesan [24] estimated the finite difference solution for the same formulation by incorporating inertial forces.

Density variations confronted in thermal and solutal characteristics cause the stratification of fluid motion. In general, accumulation of diffusive species with high density introduces the notion of stratification with respect to temperature and concentration of these species. Conceptualization of stratified flows addressed in the fields of geophysics, studies

on hydraulics and environmental issues (Armenio and Sarkar [2]). The numerical approximations are imperative tools in empirical modeling. Various authors admit their substantial contribution in numerical simulation of stratified flows. Stable stratification of flow in downstream direction is approximated by Himasekhar and Jaluria [15]. Srinivasan and Angirasa [35] estimated the finite difference discretization of convective thermal stratification. In accordance with Singh and Kumar [33], the chemical reaction on a stratified micro polar fluid diffuses the temperature rapidly everywhere on the permeable plate. Ganesan et al. [10] explored the stratification in dual case subject to thermophoresis on a plate. It was discerned that the stratification parameters slow down the wall shear effects near the surface.

Visco-plastic fluids manifest the reduction in consistency of the fluid, exerting high amount of shear stress on the fluid layers. This complex behaviour was modeled by Casson. This model exhibits an infinitely elevated shear rate with respect to less viscosity and low shear rate for an infinite apparent viscosity. Also, the model delineates the association of shear rate with shear stress, which is an essential measurement in blood flow characterization, and processing industries such as food stuffs, molten chocolates, etc. (Chhabra and Richardson [5]).

As Casson model is one of the frequently used models among visco-plastic fluids, research has been progressed based on this shear thinning behaviour. Shehzad et al. [31] quantified the homotopic solution and its convergence for a chemically reacting Casson fluid in homogeneous phase; whereas Sheikh and Abbas [32] extended the study to heterogeneous case for a stagnation point flow of Casson fluid on a stretching or shrinking surface. It is noted that the Runge–Kutta–Fehlberg method, together with shooting technique, render the unique solution for stretching and dual solution for shrinking specifications. Exact solution for a MHD Casson fluid flow over a plate with oscillations was evaluated by Hari et al. [13, 14]. When stratified Casson fluid flow is exposed to chemical reaction, it exhibits significant impact on the regulating properties of the fluid. The chemical reaction and solutal stratification diminish the mass diffusion of Casson fluid flow on a stretching cylinder in an inclined position under mixed convection (Rehman et al. [28]).

Electromagnetic flow control is indispensable in the situations, which evince the high friction to the surface and very low-pressure distribution. The electromagnetic body force regulates the flow in the case of highly conductive fluids. Free convective flow has been stabilized, while external magnetic field is imposed on a cylindrical enclosure along radial and axial directions (Mebarek-Oudina and Bessaih [20]). In the case of annulus, MHD flow with magnetic field along axial direction subdue the transfer of heat energy in little depth cavities, and radial magnetic field slow down the heat transfer in long cavities (Mebarek-Oudina and Bessaih [21]). The heat transfer component placed inside the smaller cylinder with constant heat flux induces the lesser heat transfer rate, while the size of heater is very small (Mebarek-Oudina [18]). During highly strenuous conditions, measuring the flow control using measurement and control techniques is very complicated. Contactless electromagnetic techniques are also available in practice, which considers Lorentz force as an essential part in the controlling mechanism (Weier et al. [36], Dubovikova et al. [7]). Externally applied magnetic field effects of hydrodynamic stability flows has been scrutinized by Mebarek-Oudina and Bessaih [19]. An electromagnetic

control device, which induces wall parallel Lorentz force, was constructed by Gailitis and Lielausis, which was modeled as an actuator with the electrodes and permanent magnets as strip-like arrangement. This setup is now familiarized with the notion called Riga-plate.

EMHD (electro-magneto-hydrodynamic) Lorentz force with the permeable and impermeable cases with strong suction were demonstrated in detail by Pantokratoras [25] and Pantokratoras and Magyari [26]. Approximating the mixed convective flow on the Riga-plate by adopting finite difference scheme proffered unconditionally stable results. These solutions affirm that the speed has been uplifted, while the flow is along the direction of EMHD Lorentz force (Magyari and Pantokratoras [17]). Prandtl fluid flow on an electro-magneto-hydrodynamic three-dimensional field with chemical reaction effects was inspected by Ganesh Kumar et al. [16]. The same fluid under concentration slip characterization generate less mass transfer rate subject to electromagnetic force and chemical reaction (Gireesha et al. [12]). Atlas et al. [3] modeled Cattaneo–Christov heat flux condition on a chemically reacting squeezing flow between Riga-plates, and the solutions are procured by shooting method. Variable conditions of mechanical properties have tremendous consequence in practical scenario. Shah et al. [30] performed a theoretical execution of the physical problem on stagnation point flow over Riga-plate corresponding to temperature dependent thermal conductivity.

Dependence of chemical reaction on the flow field of Newtonian fluid scrutinized by Alam and Ahammad [1]. Yet, no exploration is contributed to variable chemical reaction impact on non-Newtonian fluid. The present work prioritizes the breakage of chemical bond between atoms due to variable chemical reaction of EMHD Casson fluid flow on a permeable Riga-plate with stratification. Mesh-contour interpretation is an exclusive facet of this numerical modeling.

2 Formulation of the model

Free convective Casson fluid flow over a vertical Riga-plate with the variable chemical reaction along the flow field and stratification effects are under consideration. At the initial stage, the plate is immobile. So, the linearly stratified temperature and concentration bears the condition at ambience with zero velocity. At some time level $t^* > 0$, the plate accelerates upwards with a speed u_0 . At this time level, the temperature of the plate and concentration of the fluid at the vicinity of the plate raised to T_w^* ($> T_{\infty,x}^*$) and C_w^* ($> C_{\infty,x}^*$), respectively. Thus, the energy and mass transport confronted from the surface of the plate. Temperature and concentration diminish to asymptotic conditions, and the velocity decays to zero at the distant parts of the fluid flow. The flow direction is considered along x -axis vertically, and the transverse direction of the fluid motion is y -axis. The velocities u and v are described along vertical and transverse directions, respectively. The schematic representation of the model is illustrated in Figs. 1(a) and 1(b). Viscous dissipation effect is insignificant in the energy balance equation. The homogeneous first-order chemical reaction is under consideration, i.e., the reactants are in a same pace, and the reaction varies exponentially along fluid motion with respect to plate reference length. Variable chemical reaction is described as $k^* = k' \exp(-y/l^*)$.

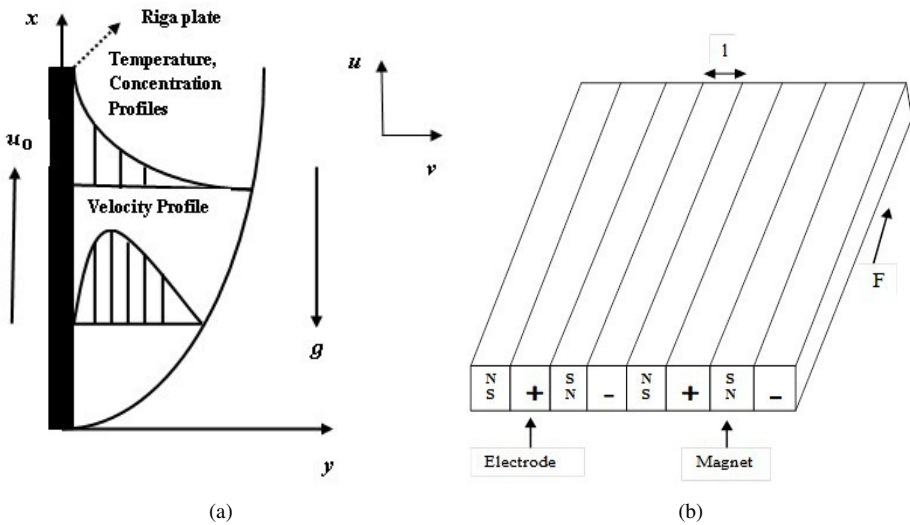


Figure 1. (a) Schematic representation of the flow model; (b) strip-wise arrangement of electrodes and magnets.

The stress strain relationship is configured as (Mustafa et al. [23], Mukhopadhyay et al. [22], Srinivas et al. [34] and Rao [27])

$$\tau_{ij} = \begin{cases} 2(\mu_b + \frac{P_y}{\sqrt{2\pi^*}})e_{ij}, & \pi^* > \pi_c^*, \\ 2(\mu_b + \frac{P_y}{\sqrt{2\pi_c^*}})e_{ij}, & \pi^* \geq \pi_c^*. \end{cases}$$

Here, $\pi^* = e_{ij}e_{ij}$, π^* is the product of shear rate components, π_c^* is the critical value of π^* , e_{ij} is the (i, j) th of component of the shear rate, μ_b and P_y are the plastic dynamic viscosity and yield stress, respectively. The mathematical model encloses the above assumptions, constitutive equation, and Boussinesq approximation can be formulated as (Gebhart and Pera [11], Ganesan and Suganthi [9] and Schlichting [29])

$$\frac{\partial u}{\partial x} + \frac{\partial v}{\partial y} = 0, \tag{1}$$

$$\frac{\partial u}{\partial t^*} + u \frac{\partial u}{\partial x} + v \frac{\partial u}{\partial y} = \nu \left(1 + \frac{1}{\beta} \right) \frac{\partial^2 u}{\partial y^2} + g\beta'(T^* - T_{\infty,x}^*) + g\beta^*(C^* - C_{\infty,x}^*) + \frac{\pi J_0 M_0 \exp(-\frac{\pi}{l}y)}{8\rho} - \frac{uv}{\lambda^*}, \tag{2}$$

$$\frac{\partial T^*}{\partial t^*} + u \frac{\partial T^*}{\partial x} + v \frac{\partial T^*}{\partial y} = \alpha \frac{\partial^2 T^*}{\partial y^2}, \tag{3}$$

$$\frac{\partial C^*}{\partial t^*} + u \frac{\partial C^*}{\partial x} + v \frac{\partial C^*}{\partial y} = D \frac{\partial^2 C^*}{\partial y^2} - k^*(C^* - C_{\infty,x}^*). \tag{4}$$

Suitable initial and boundary conditions of the problem are

$$\begin{aligned}
 t^* \leq 0, \quad u = 0, \quad v = 0, \quad T^* = T_{\infty,x}^*, \quad C^* = C_{\infty,x}^* \quad \text{for } x, y \geq 0, \\
 t^* > 0, \quad u = u_0, \quad v = 0, \quad T^* = T_w^*, \quad C^* = C_w^* \quad \text{for } y = 0, \\
 u = 0, \quad v = 0, \quad T^* = T_{\infty,0}^*, \quad C^* = C_{\infty,0}^* \quad \text{for } x = 0, \\
 u \rightarrow 0, \quad T^* \rightarrow T_{\infty,x}^*, \quad C^* \rightarrow C_{\infty,x}^* \quad \text{as } y \rightarrow \infty,
 \end{aligned}
 \tag{5}$$

where, ν is the kinematic viscosity, Gr is thermal Grashof number, Gc is solutal Grashof number, g is the gravitational acceleration, J_0 is the current density, k' is the chemical reaction rate, k^* is the local chemical reaction rate, l is the width of the magnets and electrodes, l^* is the reference length, M_0 represents the magnetization of the magnets, ρ is the density, λ^* is the permeability and $\alpha, D, \beta', \beta^*$ denote thermal diffusivity, mass diffusivity, thermal expansion coefficient, volumetric coefficient of expansion with concentration, respectively.

Undimensioned frame work of (1)–(4) and (5) have been carried out by the following parameters:

$$\begin{aligned}
 X = \frac{xu_0}{\nu}, \quad Y = \frac{yu_0}{\nu}, \quad U = \frac{u}{u_0}, \quad V = \frac{v}{u_0}, \quad t = \frac{t^*u_0^2}{\nu}, \\
 \lambda = \frac{\lambda^*u_0^2}{\nu^2}, \quad T = \frac{T^* - T_{\infty,x}^*}{T_w^* - T_{\infty,0}^*}, \quad C = \frac{C^* - C_{\infty,x}^*}{C_w^* - C_{\infty,0}^*}, \\
 Pr = \frac{\nu}{\alpha}, \quad Sc = \frac{\nu}{D}, \quad S = \frac{\pi\nu}{lu_0}, \quad R_p = \frac{k'\nu}{u_0^2}, \quad \delta' = \frac{\nu}{u_0l^*}, \\
 Gr = \frac{\nu g \beta' (T_w^* - T_{\infty,0}^*)}{u_0^3}, \quad Gc = \frac{\nu g \beta^* (C_w^* - C_{\infty,0}^*)}{u_0^3}, \quad Ha = \frac{\pi J_0 M_0 \nu}{8\rho u_0^3}, \\
 S_T = \frac{\frac{dT_{\infty,0}^*}{dX}}{T_w^* - T_{\infty,0}^*}, \quad S_M = \frac{\frac{dC_{\infty,0}^*}{dX}}{C_w^* - C_{\infty,0}^*}.
 \end{aligned}$$

Dimensionless form of (1)–(4) and (5) are given by

$$\frac{\partial U}{\partial X} + \frac{\partial V}{\partial Y} = 0, \tag{6}$$

$$\begin{aligned}
 \frac{\partial U}{\partial t} + U \frac{\partial U}{\partial X} + V \frac{\partial U}{\partial Y} \\
 = \left(1 + \frac{1}{\beta}\right) \frac{\partial^2 U}{\partial Y^2} + GrT + GcC + Ha \exp(-SY) - \frac{U}{\lambda},
 \end{aligned}
 \tag{7}$$

$$\frac{\partial T}{\partial t} + U \frac{\partial T}{\partial X} + V \frac{\partial T}{\partial Y} = \frac{1}{Pr} \frac{\partial^2 T}{\partial Y^2}, \tag{8}$$

$$\frac{\partial C}{\partial t} + U \frac{\partial C}{\partial X} + V \frac{\partial C}{\partial Y} = \frac{1}{Sc} \frac{\partial^2 C}{\partial Y^2} - R_p \exp(-\delta'Y)C. \tag{9}$$

Appropriate initial and boundary conditions are

$$\begin{aligned}
 t \leq 0, \quad U = 0, \quad V = 0, \quad T = 0, \quad C = 0 \quad \text{for } X, Y \geq 0, \\
 t > 0, \quad U = 1, \quad V = 0, \quad T = 1 - S_T X, \quad C = 1 - S_M X \quad \text{for } Y = 0, \\
 U = 0, \quad V = 0, \quad T = 0, \quad C = 0 \quad \text{for } X = 0, \\
 U \rightarrow 0, \quad T \rightarrow 0, \quad C \rightarrow 0 \quad \text{as } Y \rightarrow \infty.
 \end{aligned} \tag{10}$$

Here $\beta = \mu_b \sqrt{2\pi_c^*} / P_y$ is the Casson parameter, λ is the permeability parameter, κ is the thermal conductivity, R_P , Ha , S_T , S_M , δ' , Pr and Sc are the chemical reaction parameter, modified Hartmann number, thermal stratification parameter, solutal stratification parameter, dimensionless length parameter, Prandtl number and Schmidt number, respectively. U , V , T and C are the respective dimensionless notions of vertical velocity component, horizontal velocity component, temperature and concentration.

3 Numerical approximation

The Prandtl boundary layer equations (6), (7), (8) and (9) with the boundary conditions (10) are nonlinear in nature and coupled. The spatial and time discretization has been adopted in the system. Each derivative in the equation is approximated with the implicit scheme of Crank–Nicolson method [4]. The variables at the new time level are coupled with the new (unknown) time level, i.e., the variables U_{ij}^{m+1} , T_{ij}^{m+1} and C_{ij}^{m+1} entail the values at $(m + 1)$ th time level. The rectangular domain is divided to form uniform cells (where $X_{\max} = 1.0$ and $Y_{\max} = 15.0$).

Grid points denote the coordinates as the spatial and time steps that are fixed with the sizes $\Delta X = 0.02$, $\Delta Y = 0.25$ and $\Delta t = 0.01$, which are determined by the solution domain of grid independence. A tridiagonal system, which is deduced from the difference equations, has been evaluated through Thomas algorithm. The absolute difference of 10^{-5} between two successive iterative steps proclaims the steady state solutions. During the computational process, the following issues must be addressed: compatibility of the scheme, stability, convergence and accuracy.

Local truncation error $O(\Delta t^2 + \Delta Y^2 + \Delta X)$ ratifies the compatibility, while $O(\Delta t^2 + \Delta Y^2 + \Delta X) \rightarrow 0$ as $\Delta X \rightarrow 0$, $\Delta Y \rightarrow 0$ and $\Delta t \rightarrow 0$. The method may encounter stability problems when the solution space is not spatially smooth, even though the scheme is implicit. Some source terms in the equations may affect the stability. However, the scheme, which is considered in this numerical simulation, is unconditionally stable, and it is assured by Von Neumann stability analysis. Stability and compatibility insinuate the convergence. Although the implicit methods necessitate more memory (for coefficients and source terms) and computational effort, the method is most efficient and accurate.

Many real time situations demand the mechanical properties such as wall shear stress, the rate of heat and mass transfer. These can be estimated by the following expressions

which encompass velocity, temperature and concentration:

$$\begin{aligned} \tau_X &= -\left(1 + \frac{1}{\beta}\right) \left(\frac{\partial U}{\partial Y}\right)_{Y=0}, & \bar{\tau} &= -\int_0^1 \left(1 + \frac{1}{\beta}\right) \left(\frac{\partial U}{\partial Y}\right)_{Y=0} dX, \\ Nu_X &= \frac{-X(\frac{\partial T}{\partial Y})_{Y=0}}{1 - S_T X}, & Sh_X &= \frac{-X(\frac{\partial C}{\partial Y})_{Y=0}}{1 - S_M X}, \\ \overline{Nu} &= \int_0^1 \frac{-(\frac{\partial T}{\partial Y})_{Y=0}}{1 - S_T X} dX, & \overline{Sh} &= \int_0^1 \frac{-(\frac{\partial C}{\partial Y})_{Y=0}}{1 - S_M X} dX. \end{aligned}$$

The two dimensional plots are figured out for the steady state solutions at $X = 1.0$. Mesh plots, together with the respective projection on 2D plane (contour slices), are framed for array of elements corresponding to various values of X, Y .

4 Discussion on the results

The stratification analysis is confined for $0 \leq S_T \leq 1$ and $0 \leq S_M \leq 1$ to measure the thermal and mass diffusion from one to zero. The variable chemical reaction addressed in this analysis encounters the exponential decrease along the reference length of the plate and the distance of the fluid flow from the plate surface. In the computational domain, the value of Y varies from $Y_{\min} = 0$ to the maximum value $Y_{\max} = 15$. Based on the boundary conditions, it is evident that the flow properties are dropped down for $Y \rightarrow \infty$. The combination of reaction rate and exponential variation with respect to distance from the plate contribute to variable chemical reaction. As the maximum value of Y is confined to 15, the dimensionless length parameter is taken as $\delta' < 15$. To investigate the destructive and constructive chemical reaction, the values of reaction rate discussed for negative and positive values.

This investigation is well comparable with the computed results of Gebhart and Pera [11]. Figure 2 provides the detailed illustration of this comparison. The visual representations have been framed via two dimensional plots as well as mesh and contour plots. The contour graphs are drawn for the contour interval of length 0.15.

The cross effect of magnetic and electric field dispenses a convincing flow control and improves the speed. Figures 3 and 4 depict the changes in the flow speed with respect to modified Hartmann number (Ha). Figure 3 imparts the analogy between the velocity field over Riga-plate and an isothermal plate, which is not constructed as an actuator. It visualizes the mesh plot of velocity distribution and its two-dimensional contour graph. An intriguing fact of this representation is that the elevations can be viewed as the three-dimensional meshes as well as the slices of 3D plot in terms of contours at equal elevation above the XY -plane. For $Ha = 0$, thickness of the velocity boundary layer is less comparing to the speed at $Ha = 1$, i.e., the flow along the main stream with the aiding effect increases the velocity. Hence, it is evident that the Riga-plate setup stimulates the speed.

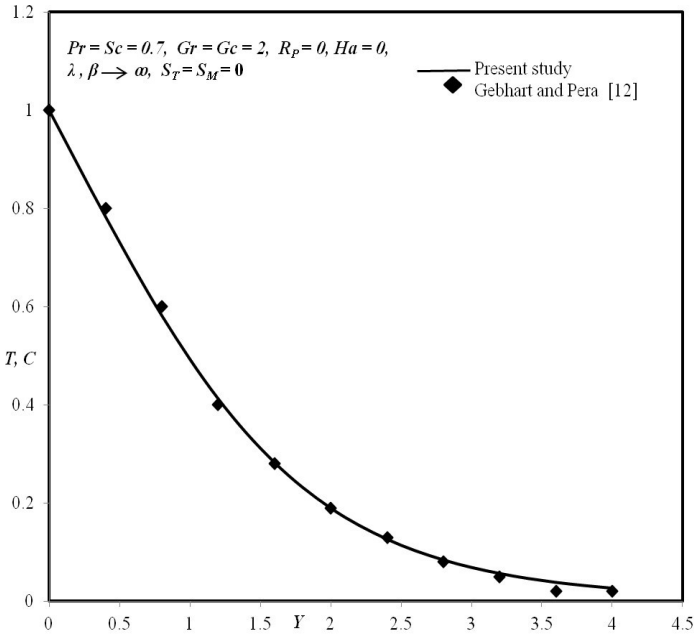


Figure 2. Comparison with the results of Gebhart and Pera.

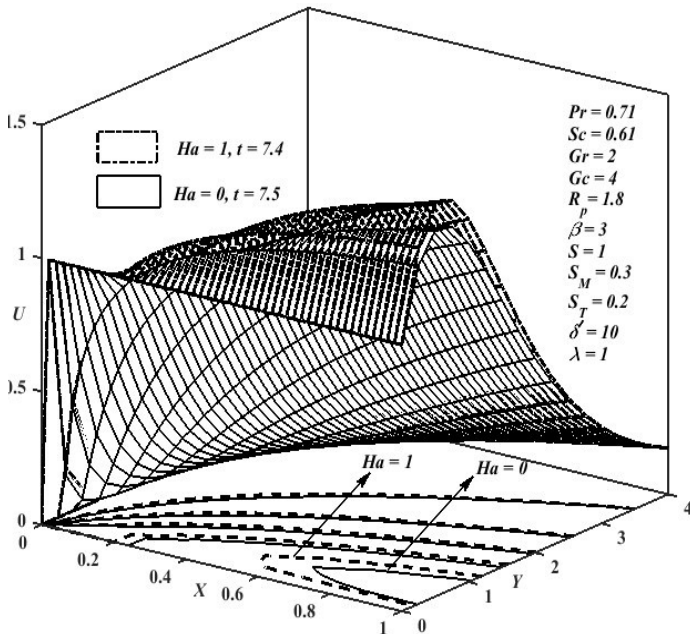


Figure 3. Mesh-contour plot of velocity.

Further, Fig. 4 also delineates the impressions of the other parameters S_T , R_p and λ . Thermal stratification strengthens the adhesion between the layers of the fluid. Thus, the higher values of stratification parameter S_T slow down the velocity; likewise, the chemical reaction parameter reduces it. The finer structure of the porous membrane shows a reduction in fluid motion, while it passes over the pores. In order that, the speed is provoked by the larger permeability parameter.

Figures 5 and 7 expose the mesh-contour visualization of thermal and mass diffusion correlation on an isothermal plate, which does not form a Riga-plate arrangement ($Ha = 0$), and Riga-plate ($Ha = 1$). In both the graphs, it is disclosed that the mesh plot for $Ha = 0$ suppress the mesh layer of $Ha = 1$. Also, the wider contour slices for $Ha = 0$ and comparatively wispiest slices for $Ha = 1$ have been portrayed. That is, the stronger electro magnetization of the setup substantially exhibits the drop in thermal and mass diffusion over the Riga-plate. A similar argument is also manifested in Figs. 6 and 8 for Ha .

The explication of temperature distribution for S_T and R_p is elucidated in Fig. 6. The chemical reaction, which is under consideration, is depending on the length of the plate and the region of the fluid motion, which is far away from the surface. The heightened values of chemical reaction parameter enhances the temperature. Because, the faster chemical reaction causes the rapid collision of molecules in the fluid flow. Stratification precipitates the consistency of the fluid, which weakens the energy transport in fluid motion. Hence, temperature drops down to lower level.

The mass diffusive attributes of the flow have been expounded in Fig. 8. By virtue of stratification, the density differences cause the layer deposition along the height of the plate. Hence, raising the values of mass stratification parameter diminishes the concentration of the fluid flow. Chemical reaction is taken as an exponential function, which is decaying along the fluid motion. The stronger reaction rate of the reactants with respect to diffusive species reduces the consistency of the fluid. Thus, the improved values of R_p deteriorates concentration.

Skin friction has been investigated in Figs. 9 and 10 for local and average sense. The continual enlargement in size of the pores, which surrounds the plate allows the fluid to get pass over it rapidly, so that the friction on the surface of the plate declines. By this way, larger permeability parameter (λ) values reduce τ_X , although the chemical reaction parameter raises it. Moreover, the flow along main stream velocity speed up the fluid motion with higher modified Hartmann number (Ha) values. Stratification with respect to temperature and concentration aligns the fluid layers based on the density differences. This results in the reduction of viscous drag for escalated S_T and S_M .

Heat transfer rate simulation is attempted in Figs. 11 and 12 for local and mean values. Thermal and mass stratification necessitates the energy supply to attain the stable level. This energy emanates from the thermal, mass and gravitational physical aspects. At the peak, stratification parameters disclose the reduction in Nusselt number values. Magnetization of the magnets is affected by the heat energy. Thus, Magnetic field strength slow down the rate of heat transfer while exalting Ha . Similarly, chemical reaction parameter lessens the Nusselt number. Contrary to this, raise in λ enhances rate of heat transfer.

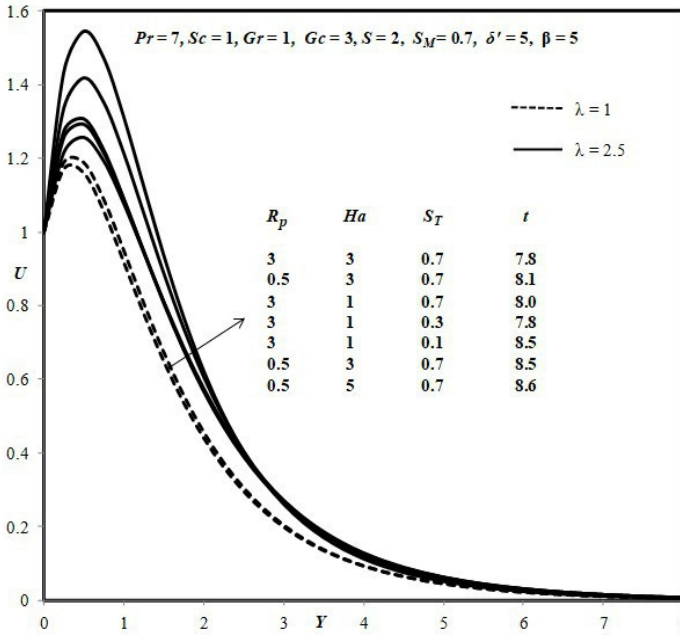


Figure 4. Velocity distribution in the flow field for variations in R_p, Ha, S_T and λ .

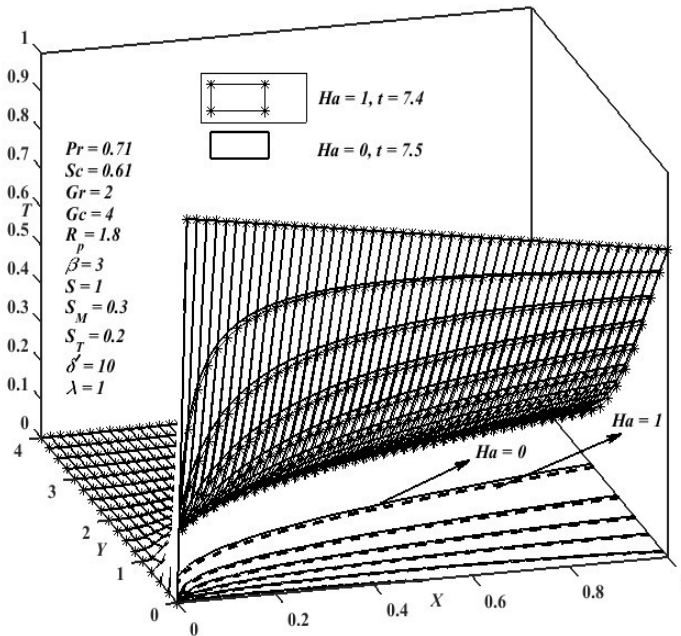


Figure 5. Mesh-contour plot of temperature.

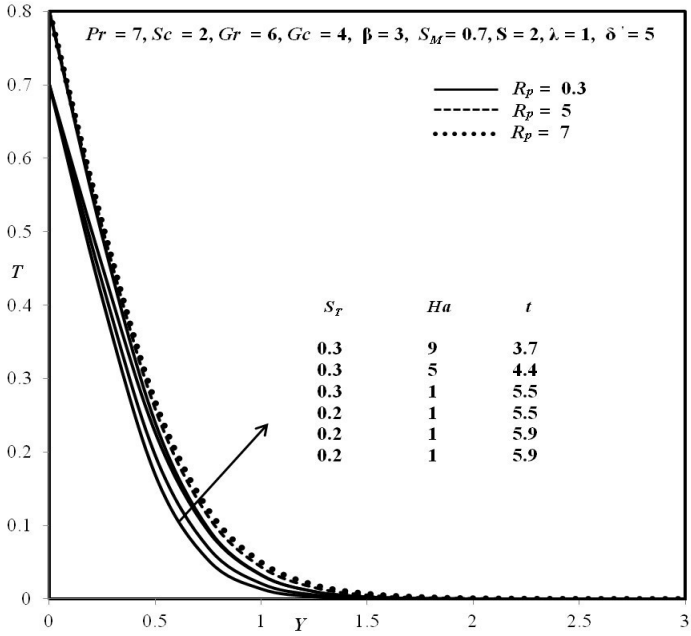


Figure 6. Temperature distribution for variations in R_p, Ha and S_T .

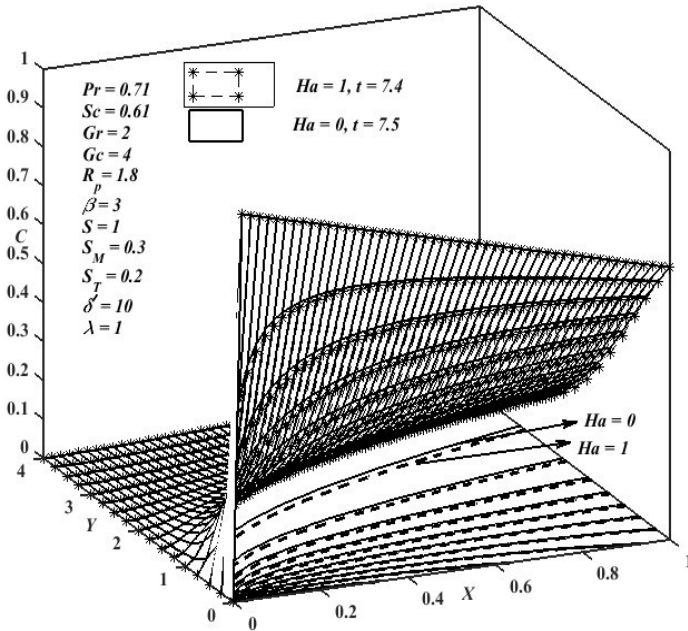


Figure 7. Mesh-contour plot of concentration.

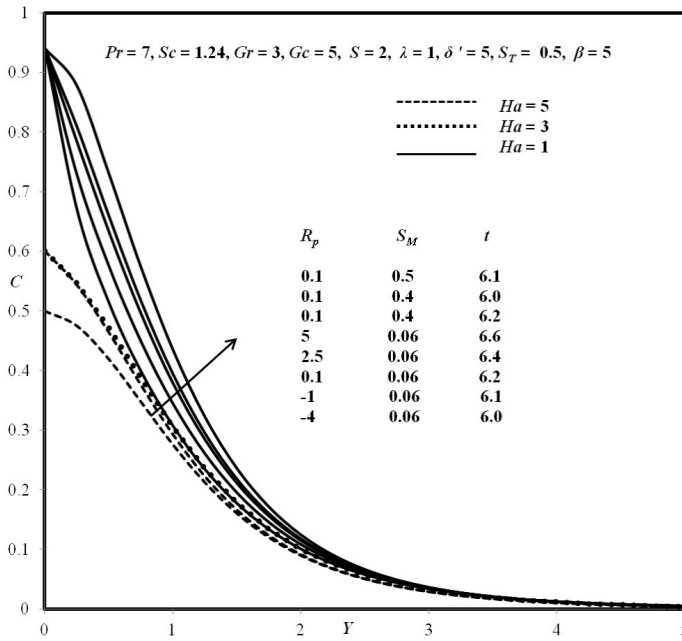


Figure 8. Concentration distribution for variations in R_p , Ha and S_M .

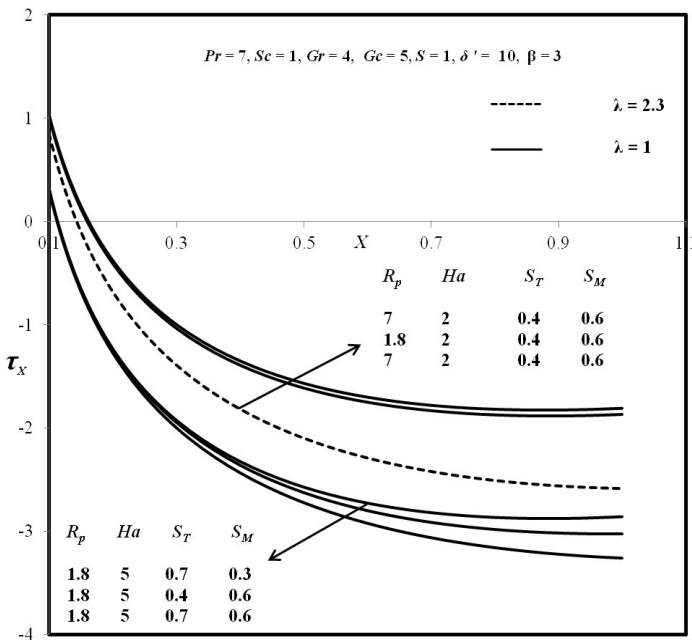


Figure 9. Local shear stress on the surface.

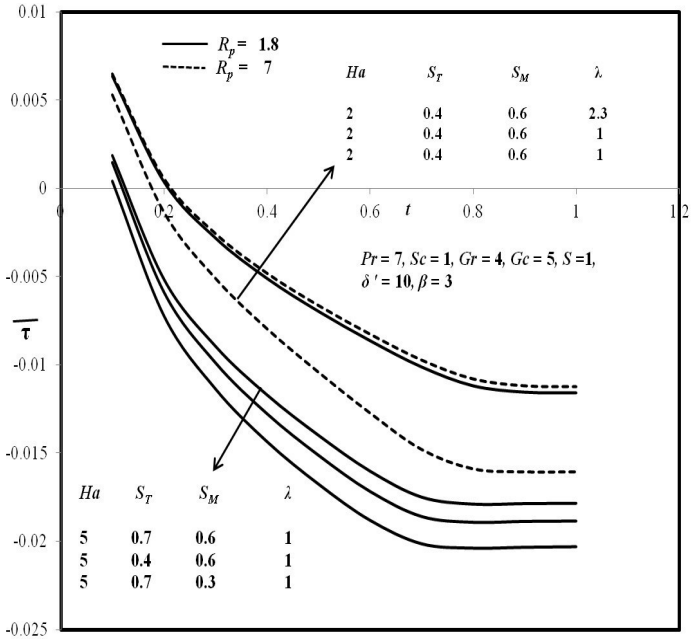


Figure 10. Mean shear stress on the surface.

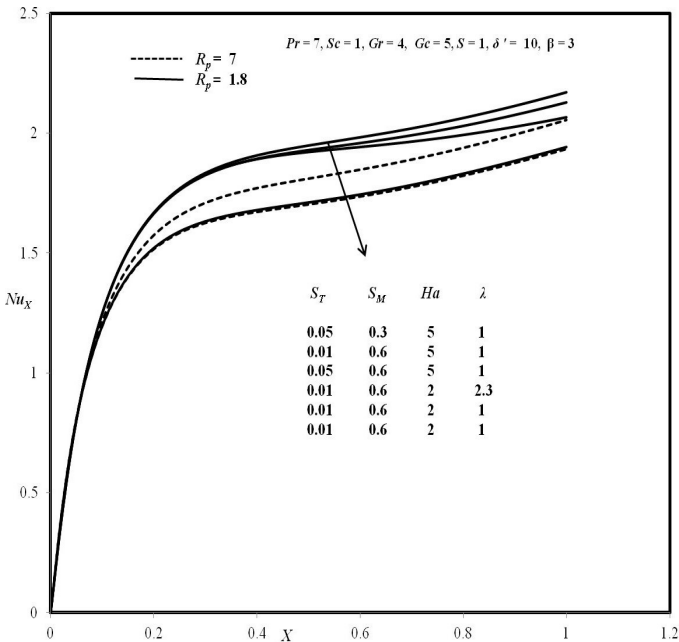


Figure 11. Rate of heat transfer in local sense.

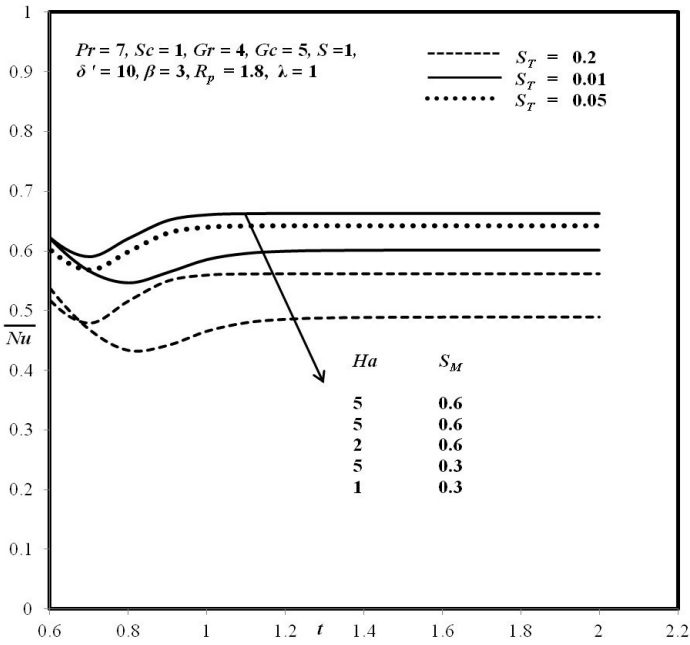


Figure 12. Mean heat transfer rate in the fluid flow.

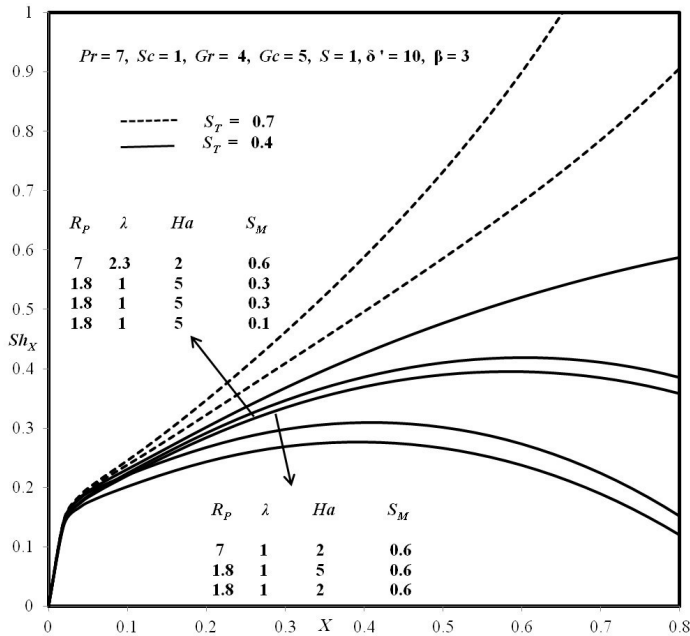


Figure 13. Rate of mass transfer in local sense.

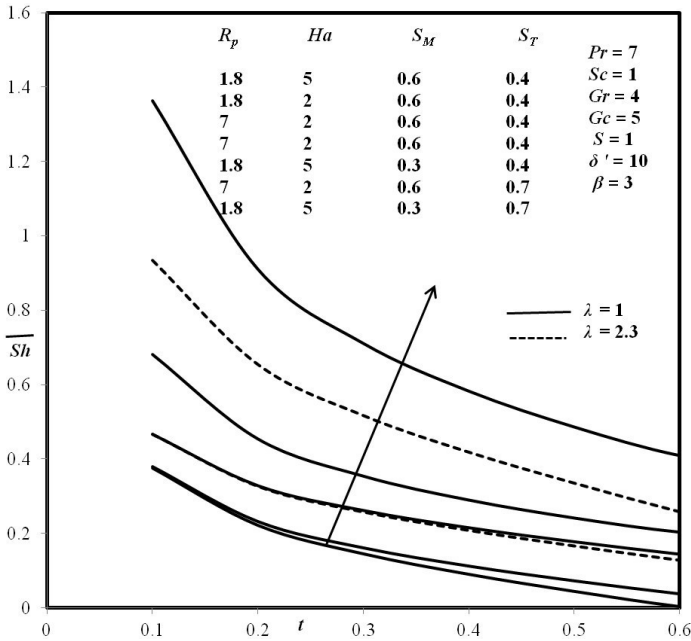


Figure 14. Mean mass transfer rate.

Deviations pertaining to Sherwood number demonstrated in Figs. 13 and 14. Higher reaction rate instigates the breakage of bond between atoms during chemical reaction. These circumstances enhance the mass transfer rate, i.e., larger R_p values elevate Sherwood number values. Mass stratification aligns the layer of fluid according to density variations, which shows the reduction in concentration gradient. Thus, the incremental change in S_M weakens the mass transfer rate; whereas S_T boost up the Sherwood number values. Heightened values of Ha intensify the rate of mass transfer due to electrical conductivity and magnetic effects, but the permeability parameter lessens it.

5 Conclusions

Significance of variable properties on real time applications is evident. The most incentive part of this investigation is that the exponential form of chemical reaction rate and it carry out the Casson fluid flow past a Riga-plate with variable chemical reaction and stratified conditions. The following culminations are confronted:

- Velocity shows a significant improvement when the fluid flow on the Riga-plate.
- The stronger variable chemical reaction along the fluid flow escalates the mass transfer rate. It declines the velocity nevertheless.
- The heat transfer rate monotonically increases, while the stratification is uplifted along the height of the plate in thermal and mass stratified conditions.

- Permeability parameter boosts up the velocity and reduces the shear stress on the surface.
- The large amount of mass stratification slows down the rate of mass transfer in the fluid motion.
- Intensity of temperature and concentration distribution is lower in the fluid flow on a Riga-plate

Acknowledgment. One of the authors, K. Deepa, immensely expresses her gratitude to Anna University, Chennai, for supporting this research work through “Anna Centenary Research Fellowship”.

References

1. M.S. Alam, M.U. Ahammad, Effects of variable chemical reaction and variable electric conductivity on free convective heat and mass transfer flow along an inclined stretching sheet with variable heat and mass fluxes under the influence of dufour and soret effects, *Nonlinear Anal. Model. Control*, **16**(1):1–16, 2011.
2. V. Armenio, S. Sarkar, *Environmental Stratified Flows*, Springer, New York, 2005.
3. M. Atlas, S. Hussain, M. Sagheer, Entropy generation and squeezing flow past a Riga plate with Cattaneo–Christov heat flux, *Bull. Pol. Acad. Sci., Tech. Sci.*, **66**(3):291–300, 2018.
4. B.Carnahan, H.A. Luther, J.O. Wilkes, *Applied Numerical methods*, John Wiley & Sons, New York, 1969.
5. R.P. Chhabra, J.F. Richardson, *Non-Newtonian Flow in the Process Industries: Fundamentals and Engineering Applications*, Butterworth-Heinemann, Oxford, 1999.
6. U.N. Das, R. Deka, V.M. Soundalgekar, Effects of mass transfer on flow past an impulsively started infinite vertical plate with constant heat flux and chemical reaction, *Forsch. Ingenieurwesen*, **60**(10):284–287, 1994.
7. N. Dubovikova, C. Karcher, C. Kolesnikov, Electromagnetic flow control in liquid metals using Lorentz force techniques, *PAMM, Proc. Appl. Math. Mech.*, **14**:721–722, 2014.
8. P. Érdi, J. Tóth, *Mathematical Models Of Chemical Reaction. Theory and Applications of Deterministic and Stochastic Models*, Manchester Univ. Press, Manchester, 1989.
9. P. Ganesan, R.K. Suganthi, Free convective flow over a vertical plate in a doubly stratified medium with electrophoresis, heat source/sink and chemical reaction effects, *Korean J. Chem. Eng.*, **30**(4):813–822, 2013.
10. P. Ganesan, R.K. Suganthi, P. Loganathan, Thermophoresis particle deposition effects in a free convective doubly stratified medium over a vertical plate, *Meccanica*, **49**:659–672, 2014.
11. B. Gebhart, L. Pera, The nature of vertical natural convection flows resulting from the combined buoyancy effects of thermal and mass diffusion, *Int. J. Heat Mass Transfer*, **14**:2025–2050, 1971.
12. B.J. Gireesha, K. Ganesh Kumar, B.C. Prasannakumar, Scrutinization of chemical reaction effect on flow and mass transfer of Prandtl liquid over a Riga plate in the presence of solutal slip effect, *Int. J. Chem. Reactor Eng.*, **16**(8), 2018.

13. R.K. Hari, R.P. Harshad, Heat and mass transfer in magnetohydrodynamic (MHD) Casson fluid flow past over an oscillating vertical plate embedded in porous medium with ramped wall temperature, *Propul. Power Res.*, **7**(3):257–267, 2018.
14. R.K. Hari, H.K. Patel, Radiation and chemical reaction effects on MHD Casson fluid flow past an oscillating vertical plate embedded in porous medium, *Alexandria Eng. J.*, **55**(3):583–595, 2016.
15. K. Himasekhar, Y. Jaluria, Laminar buoyancy-induced axisymmetric free boundary flows in a thermally stratified medium, *Int J Heat Mass Transfer*, **25**:213–221, 1982.
16. K. Ganesh Kumar, R. Haq, N.G. Rudraswamy, B.J. Gireesha, Effects of mass transfer on MHD three dimensional flow of a Prandtl liquid over a flat plate in the presence of chemical reaction, *Results Phys.*, **7**:3465–3471, 2017.
17. E. Magyari, A. Pantokratoras, Aiding and opposing mixed convection flows over the Riga-plate, *Commun. Nonlinear Sci. Numer. Simul.*, **16**:3158–3167, 2011.
18. F. Mebarek-Oudina, Numerical modeling of the hydrodynamic stability in vertical annulus with heat source of different lengths, *Eng. Sci. Technol.*, **20**:1324–1333, 2017.
19. F. Mebarek-Oudina, R. Bessaih, Effects of the geometry on the MHD stability of natural convection flows, in *Topical Problems of Fluid Mechanics, Vol. 75*, Institute of Thermomechanics AS CR, v.v.i., 2014, pp. 159–161.
20. F. Mebarek-Oudina, R. Bessaih, Numerical modeling of MHD stability in a cylindrical configuration, *J. Franklin Inst.*, **351**:667–681, 2014.
21. F. Mebarek-Oudina, R. Bessaih, Oscillatory magnetohydrodynamic natural convection of liquid metal between vertical coaxial cylinders, *J. Appl. Fluid Mech.*, **6**(4):1655–1665, 2016.
22. S. Mukhopadhyay, P. Ranjan De, K. Bhattacharyya, G.C. Layek, Casson fluid flow over an unsteady stretching surface, *Ain Shams Eng. J.*, **4**:933–938, 2013.
23. M. Mustafa, T. Hayat, I. Pop, A. Aziz, Unsteady boundary layer flow of a Casson fluid due to an impulsively started moving flat plate, *Heat Transfer Asian Res.*, **40**(6):563–576, 2011.
24. R. Muthucumaraswamy, P. Ganesan, On impulsive motion of a vertical plate with heat flux and diffusion of chemically reactive species, *Forsch Ingenieurwesen*, **66**:17–23, 2000.
25. A. Pantokratoras, Some exact solutions of boundary layer flows along a vertical plate with buoyancy forces combined with Lorentz forces under uniform suction, *Math. Probl. Eng.*, **2008**:149272, 2008.
26. A. Pantokratoras, E. Magyari, EMHD free-convection boundary-layer flow from a Riga-plate, *J. Eng. Math.*, **64**:303–315, 2009.
27. M.E. Rao, The effects of thermal radiation and chemical reaction on MHD flow of a Casson fluid over and exponentially inclined stretching surface, *J. Phys., Conf. Ser.*, **1000**:2997–3006, 2017.
28. K.U. Rehman, A.A. Malik, M.Y. Malik, N. Sandeep, N.U. Saba, Numerical study of double stratification in Casson fluid flow in the presence of mixed convection and chemical reaction, *Results Phys.*, **7**:933–938, 2013.
29. H. Schlichting, *Boundary Layer Theory*, Wiley, New York, 1979.
30. S. Shah, S. Hussain, M. Sagheer, Impacts of variable thermal conductivity on stagnation point boundary layer flow past a Riga plate with variable thickness using generalized Fourier's law, *Results Phys.*, **9**:303–312, 2018.

31. S.A. Shehzad, T. Hayat, M. Qasim, S. Asghar, Effects of mass transfer on MHD flow of Casson fluid with chemical reaction and suction, *Braz. J. Chem. Eng.*, **30**:187–195, 2013.
32. M. Sheikh, Z. Abbas, Homogeneous–heterogeneous reactions in stagnation point flow of Casson fluid due to a stretching/shrinking sheet with uniform suction and slip effects, *Jordan Journal of Mechanical and Industrial Engineering*, **9**(4):279–288, 2015.
33. K. Singh, M. Kumar, The effect of chemical reaction and double stratification on MHD free convection in a micropolar fluid with heat generation and Ohmic heating, *Results Phys.*, **9**:303–312, 2018.
34. S. Srinivas, C.K. Kumar, A.S. Reddy, Pulsating flow of Casson fluid in a porous channel with thermal radiation, chemical reaction and applied magnetic field, *Nonlinear Anal. Model. Control*, **23**(2):213–233, 2018.
35. J. Srinivasan, D. Angirasa, Numerical study of double-diffusive free convection from a vertical surface, *Int. J. Heat Mass Transfer*, **31**:2033–2038, 1982.
36. T. Weier, G. Gerbeth, G. Mutschke, O. Lielausis, G. Lammers, Control of flow separation using electromagnetic forces, *Flow Turbul. Combust.*, **71**:5–17, 2003.